J Mater Sci (2010) 45:2062–2070
DOI 10.1007/s10853-009-4066-7

HTC2009

# The effect of carbon nanolayers on wetting of alumina by NiSi alloys

**A. Koltsov · A. Crisci · F. Hodaj · N. Eustathopoulos**

Received: 12 June 2009 / Accepted: 22 November 2009 / Published online: 11 December 2009
© Springer Science+Business Media, LLC 2009

**Abstract** Ionocovalent oxides such as alumina, silica or magnesia are not wetted by Si and Si-rich alloys, the contact angles being close to 90°. The aim of this work is to study the effect of submicron carbon layers on wetting in this type of system. In principle, silicon reacts with carbon to form silicon carbide, a compound wettable by Si alloys. However, the formation of silicon carbide at the interface can be affected by the dissolution of this compound into the molten alloy occurring in order to saturate the melt in carbon. These phenomena are studied using a model system consisting of Ni–63 at.%Si alloy and monocrystalline alumina substrate coated with carbon layers. Wetting experiments are performed by the dispensed drop technique in high vacuum varying the parameters: thickness of coating (from 0 to 100 nm), temperature and degree of carbon saturation of the alloy. The surfaces and reactive interfaces are characterised by SEM, X-ray microanalysis and XPS.

## Introduction

Pure Si and Si-based alloys wet various non-oxide ceramics, such as SiC, $Si_3N_4$, C or again AlN (contact angle $\theta \ll 90°$ [1]) and can be used for brazing these ceramics (see for example Ref. [2]). However, these alloys do not wet oxide ceramics such as alumina, silica or magnesia, the contact angle being close to or higher than 90° [1]. The aim of this work is to study the effect of thin carbon layers on the oxide on wetting in this type of system.

The idea of improving wetting in a carbide-forming metal/oxide system by carbon coating is not new. Twenty years ago John and Hausner [3] attempted to improve wetting of Al on monocrystalline alumina by depositing thin carbon layers a few tens of nm thick on the alumina surface. In this way, the contact angle $\theta$ of Al in a vacuum of $4 \times 10^{-5}$ Pa at 700° was 85°, more than 35° lower than the value of 122° observed on uncoated alumina. At 1000 °C the difference between these two types of angle was 15°–20°. The authors reported the formation of very small crystals at the interface, supposed to be Al carbide or Al oxicarbide ($Al_2OC$ or $Al_4O_4C$), and attributed the beneficial effect of carbon on wetting these compounds. However, the results of these authors, especially those obtained at 700 °C, where the contact angle of clean Al is close to 90°, strongly suggest that a large part of the decrease in $\theta$ comes from a beneficial effect of carbon in Al deoxidation.

Weirauch and Krafick [4] also studied the effect of 100–200 nm thick carbon layers on $Al_2O_3$ on wetting by Al at 950 °C in a vacuum of $10^{-2}$ Pa. After long-term holding at this temperature (24 h), the contact angles on uncoated alumina observed in two experiments were 63° and 71° while three experiments with coated alumina gave values of 35°, 31° and 61°. No direct evidence of a new phase at the Al/C-coated alumina interface was obtained. The beneficial effect of carbon coatings on wetting was attributed to the dissolution of carbon into Al and/or to the formation

A. Koltsov · F. Hodaj · N. Eustathopoulos
SIMaP-UMR CNRS 5266, Grenoble INP-UJF, BP 75,
38402 Saint Martin d'Hères, France

A. Koltsov (✉)
ArcelorMittal Research S. A., Voie Romaine BP 30320,
57283 Maizières-Lès-Metz, France
e-mail: alexey.koltsov@arcelormittal.com

A. Crisci
CMTC, Grenoble INP-UJF, BP 75, 38402 Saint Martin d'Hères,
France

of Al carbide. Note that $\theta$ values as low as 30–35° measured with coated alumina are much lower than the contact angles of 70–75° observed by John and Hausner [3] for coated alumina at 1000 °C. Moreover, the values of 30–35° are even lower than the contact angles observed in the same study with bulk graphite (54° and 57°). It is possible that evaporation of Al occurring in high vacuum may affect contact angle measurements in long-term experiments.

In a recent study, Sobczak et al. [5] found that, at 1000 °C in a vacuum of $10^{-4}$ Pa, the contact angle of Al on alumina coated by a 1 μm thick carbon layer is 78°, which is 10–15° lower than on uncoated alumina, in good agreement with the findings of John and Hausner.

To summarise, the three mentioned studies have shown a significant improvement in alumina wetting by Al resulting from C coatings. However, the mechanism involved in this improvement has not yet been determined. A reason for this is the well known difficulty in wetting experiments arising from Al oxidation [1]. A further reason is the absence in the above studies of direct characterisation of the interface.

The aim of this study is to determine the fundamental issues of wetting of C-coated alumina (and more generally of ionocovalent oxides) by carbide-forming alloys. The system chosen for this study is a model system consisting of the Ni–63 at.%Si alloy and monocrystalline alumina. Like Al, molten Si reacts with carbon to form SiC, which is a predominantly covalent ceramic wettable by liquid metals [1, 6]. The advantage of Ni–63 at.%Si alloy is that its wetting behaviour on bulk C substrates is known and well understood [7, 8]. A point experiment was performed with a Zr–Si alloy. A difficulty arising when working with Si alloys is that these alloys, such as Al, are also oxidisable. In the present study, this difficulty is overcome using the 'dispensed drop' version of the sessile drop technique.

## Experimental procedure

The nickel–silicon alloys used are prepared from pure Ni (99.997 wt%) and Si (99.9995 wt%) by melting and alloying in an alumina crucible during experiments performed in high vacuum ($10^{-5}$ Pa). The Zr–10 at.%Si alloys are prepared in situ, by direct melting in high vacuum of the appropriate quantities of $ZrSi_2$ (99.5%) and Si (99.5%) powders.

High purity (99.995%) α-alumina single crystals with a randomly oriented surface were used. Their surface was polished to an average roughness of about 1 nm measured by high resolution optical profilometry.

Wetting was studied by the 'dispensed drop' method, which is derived from the classical sessile drop technique, in a metallic furnace under a vacuum of $5 \times 10^{-5}$ Pa. The apparatus consists essentially of a molybdenum heater surrounded by molybdenum radiation shields, located in a water-cooled stainless-steel chamber. The chamber is fitted with two windows enabling the illumination of the sessile drop on the substrate.

The drop images were produced using an optical system fitted with a zoom (magnification ×30). The time-dependent change in linear dimension (drop base radius $R$) and contact angle $\theta$ of the drop were filmed by a CCD video camera and recorded on videotape at a film speed of 25 frames per second. After the experiment, $\theta$ and $R$ were measured from the drop profile using a drop shape analysis software with an accuracy of ±2° for $\theta$ and ±1% for $R$.

Once the experiment temperature is attained, the liquid is extruded from the crucible and deposited on the substrate surface, and spreading then occurs as in the classical sessile drop configuration. The main advantage of this technique is that it allows the process of melting and spreading to be separated so that fully isothermal experiments can be performed. Another advantage is that, during extrusion, any oxide layer on the liquid surface alloy is broken.

After the experiments, the drop and substrate surfaces, as well as the metal/ceramic interface were characterised by optical and electronic microscopy and by X-ray photoelectron spectroscopy (XPS).

Carbon deposition on alumina was performed by evaporation of a carbon braid under vacuum ($10^{-2}$ mbar). For a given evaporation time, the thickness of the deposited carbon layer was varied by varying the distance between the carbon source and the substrate. The carbon layers are deposited simultaneously on an alumina substrate and on a monocrystalline silicon substrate used as a reference sample in order to measure the carbon layer thickness.

The carbon layer thickness is measured by electron probe micro-analysis (EPMA). Here, the method used is based on the relation existing between the layer thickness and the ratio $k_{ratio} = I_{sample}/I_{reference}$, where $I$ is the intensity of the Si line ($SiK_\alpha$). In order to probe more or less the deposited carbon layer and the silicon substrate and so to obtain different $k_{ratio}$ for each sample, EPMA measurements were carried out using various accelerating voltages (between 3 and 5 kV). Under these conditions of analysis, the probe volume is lower than 0.12 $\mu m^3$ at 5 kV.

For carbon layers more than 50 nm thick, their thickness is also measured by high resolution optical profilometry. The difference in layer thickness obtained by these methods is 15%.

## Results

### Typical curves

A plot of the variation in contact angle $\theta$ and droplet base radius $R$ versus time for an experiment conducted at

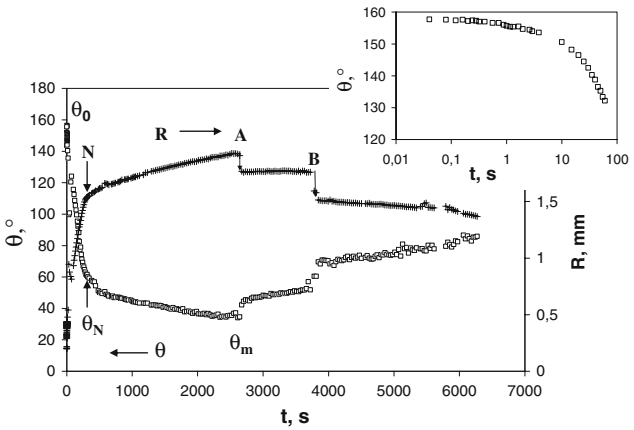


**Fig. 1** Contact angle $\theta$ and drop base radius $R$ versus time curves for the Ni–63 at.%Si alloy on carbon-coated alumina at 1200 °C. Carbon layer thickness $e = 84$ nm, mass drop $m = 17$ mg

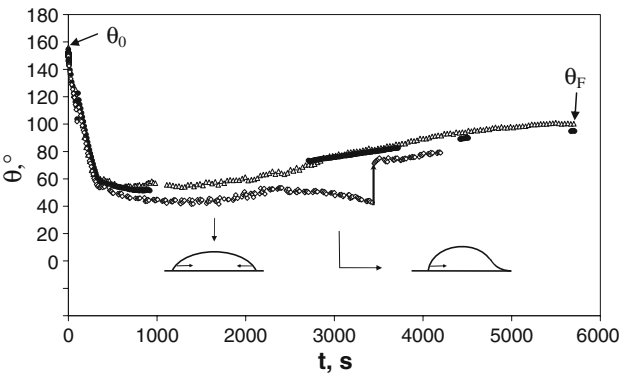


**Fig. 2** Variation in contact angle $\theta$ with time for an Ni–63 at.%Si alloy droplet ($m = 31 \pm 5$ mg) on carbon-coated alumina at 1200 °C. Three sets of data are included to show the reproducibility of the data. In one of these data sets the droplet process was not filmed continuously. Carbon layer thickness $e = 14 \pm 4$ nm

1200 °C for a Ni–63 at.%Si alloy by the dispensed drop technique is given in Fig. 1. The carbon layer thickness deposited in alumina is 84 nm.

The contact angle in this system varies non-monotonically between 180° and a contact angle close to 90° observed after 6200 s. Note that when the experiment was stopped, the contact angle was not steady but continued to increase very slowly. The spreading regime between 180° and the first measured contact angle of 156°, noted $\theta_0$, is too fast to be followed by the CCD camera used in this study with a time resolution of 40 ms. Thereafter, the contact angle decreases, first rapidly (from $\theta_0$ to $\theta_N$, where the contact angle changes from 156° to about 50°), then more slowly (from $\theta_N$ to $\theta_m = 38°$).

After $\theta = \theta_m$, a receding regime of the droplet triple line is observed with existence of triple line jumps. During this receding regime the contact angle increases from $\theta_m$ to the last measured contact angle of 90°. Hereafter, $\theta_m$ is called the minimum contact angle.

## Reproducibility of results

Figure 2 presents the $\theta(t)$ curves obtained in three different experiments performed for the same alloy composition and mass droplet at 1200 °C, and for the same carbon layer thickness $e = 14 \pm 4$ nm.

The values of initial $\theta_0$ and final or steady $\theta_F$ contact angles observed for these three experiments are well reproducible with $\theta_0 = 152 \pm 4°$ and $\theta_F = 98 \pm 3°$. As for the minimum contact angle $\theta_m$, this varies from 54 to 42°.

Although the final contact angle $\theta_F$ is the same for these three experiments, the paths followed by the drops in order to attain $\theta_F$ may be different as shown by the existence, in one experiment, of triple line pinning followed by jumping (see Fig. 2).

## Characterisation

For all samples cooling at room temperature leads to interfacial rupture as shown schematically in Fig. 3a. Both contact surfaces, i.e. the alumina side and the alloy side (noted 1 and 2, respectively, in Fig. 3a) could thus be characterised. XPS was used for this purpose in two cases, before the drop recedes, $t < t_m$ ($\theta > \theta_m$) and after complete receding of the drop, $t > t_F$.

Taking into account the fact that the lateral resolution of the XPS technique (noted by $d_{analyse}$ in Fig. 3a) is greater than the dimensions of the zone to be analysed (noted by $D_{drop}$), the analysed zone on the alumina side contains not only the part which has contacted the liquid alloy, but also a part covered by the carbon layer.

In the case where the experiment was stopped just before the contact angle has attained $\theta_m$ (see Fig. 1) the characterisation of surface 1, shows only the presence of C, Al and O but not Si. The analysis of surface 2 clearly shows the presence of Ni and Si but in this case the Si signal may be due to Si in the Ni–Si alloy as well as to SiC. The evidence of SiC formation is given by carbon peak situated at E ≈ 281.5 eV (see Fig. 3b) which is characteristic of SiC [9]. Note that the peak at E ≈ 285 eV in this figure is typical of carbon pollution produced during sample transfer from the wetting furnace to the XPS chamber. This characterisation shows that SiC is present at the interface at $t < t_m$ and that the drop detachment observed during cooling occurred at the SiC/alumina interface, not at the Ni–Si/SiC interface.

The same type of analyses performed on the alloy side of a drop in the case where complete receding has occurred, i.e. at $t > t_F$, shows the absence of the carbide peak at E ≈ 281.5 eV (see Fig. 3c).

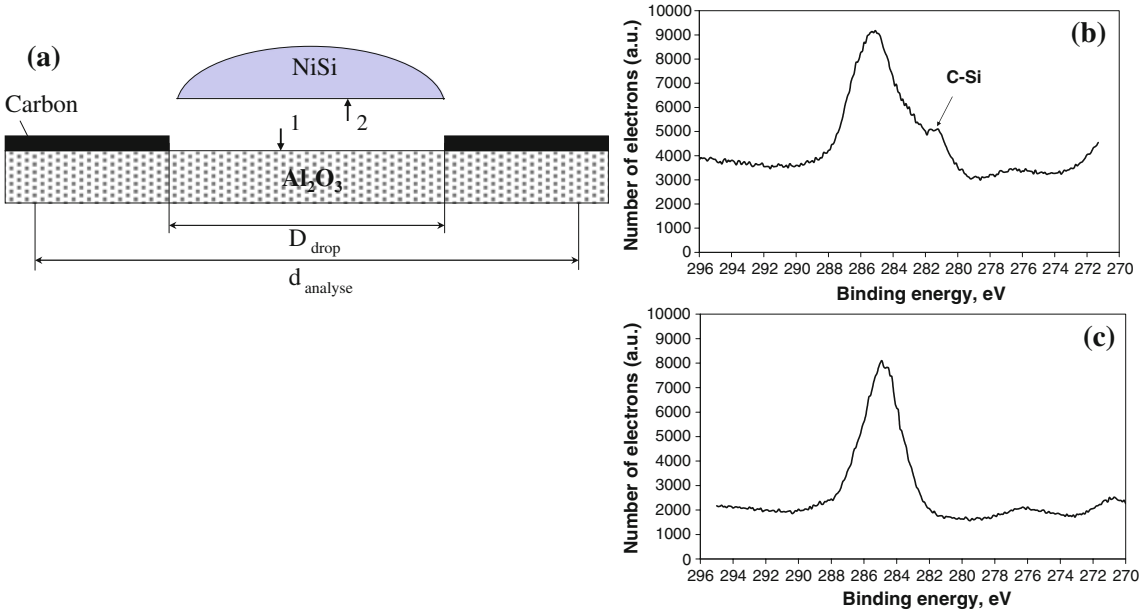


**Fig. 3** **a** Schematic presentation of surfaces (1 and 2) analysed by XPS. **b** and **c** XPS spectra of surface 2 for two different experiments: **b** the experiment is stopped just before $t_m$ (see Fig. 1) and **c** after complete dewetting ($t > t_m$). The extra peak at $E \approx 281.5$ eV in **b** is characteristic of SiC [9]

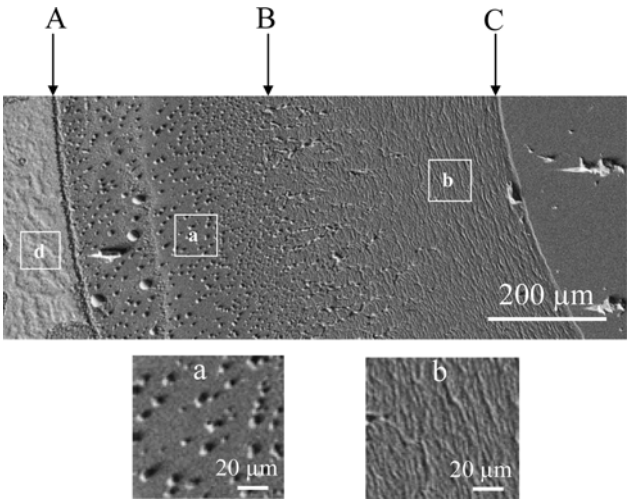


**Fig. 4** SEM micrograph, taken from above, of the substrate surface after complete dewetting of the drop (backscattered electron image). The wetting and dewetting kinetics corresponding to this experiment are described in Fig. 1. The letters A, B and C correspond to those indicated in Fig. 1

Figure 4 is a plan view of the substrate surface after complete dewetting of the drop. The letters indicated in this figure correspond to those of Fig. 1. The triple line has receded from A ($\theta = \theta_m$) to C ($\theta = \theta_F$) and two different zones can be distinguished in this area: zone *a* from A to B which contains micrometric droplets and zone *b* from B to C which presents corrosion lines (rings) of alumina.

The Energy Dispersive Spectrometry (EDS) analysis of the surface substrate ahead of the triple line, area indicated by the letter *d* in Fig. 4, clearly shows the presence of Ni and Si. The spectrum also indicates the presence of carbon in this zone (elementary carbon or more likely carbon transformed into carbide).

## Reference wetting curves

In order to analyse the experimental results, two reference wetting curves with the same alloy (Ni–63 at.%Si) are needed, the first on monocrystalline alumina and the second on bulk carbon.

The contact angle on a monocrystalline alumina substrate at 1200 °C decreases rapidly from an initial value $\theta_0 \approx 110°$ and attains a steady value close to 95° in 20 s (Fig. 5a). Thereafter, oscillations of the triple line around its equilibrium position, corresponding to a variation in $\theta$ of $\pm 3°$, are observed. These oscillations are due to slight corrosion of the alumina substrate near the triple line evidenced by the formation of typical rings a few tens of nm deep (Fig. 5b). Corrosion in this system is caused by the reaction between alumina and Si with the formation of the volatile oxide SiO [10].

Figure 6 gives the experimental results obtained by Dezellus et al. [7] for the wetting of the same alloy (Ni–63 at.%Si) on a vitreous carbon substrate ($C_V$) at 1200 °C, by the same experimental technique (dispensed drop). The reaction between Si and carbon in this system leads to the formation of a continuous layer of SiC 1 µm thick [8].

As discussed in Refs. [7, 8], the contact angle in this system varies between an initial value of $\theta_0 \approx 150°$ which

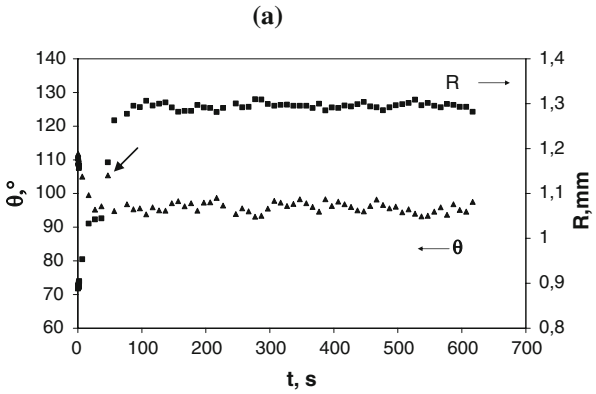


**Fig. 5** **a** Contact angle $\theta$ and drop base radius $R$ versus time curves for the Ni–63 at.%Si alloy on an alumina substrate at 1200 °C by the dispensed drop technique. The perturbation shown by an arrow on the $\theta(t)$ curve corresponds to the moment of drop detachment from the capillary. **b** Alumina surface after the wetting experiment

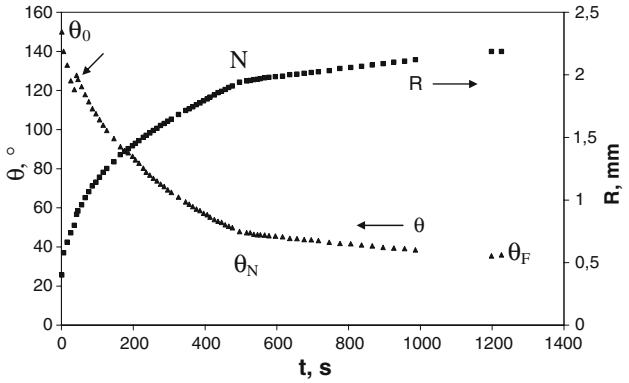


**Fig. 6** Contact angle $\theta$ and drop base radius $R$ versus time curves for the Ni–63 at.%Si alloy on a vitreous carbon substrate at 1200 °C by the dispensed drop technique [7]. The perturbation shown by an arrow on the $\theta(t)$ curve corresponds to the moment of drop detachment from the capillary

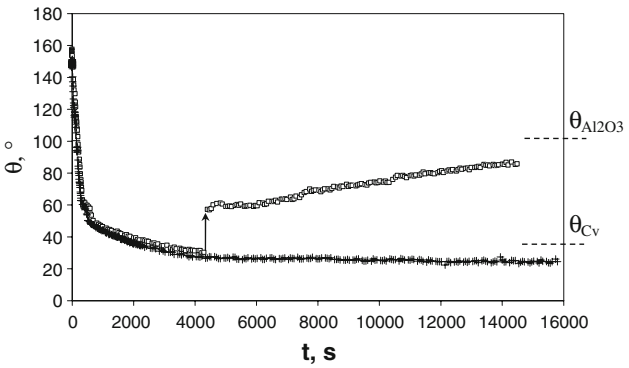


**Fig. 7** Variation in contact angle $\theta$ with time for Ni–63 at.%Si alloy droplets ($m = 50 \pm 2$ mg) on carbon-coated alumina ($e = 62 \pm 5$ nm) at 1200 °C. (+) Ni–Si alloy presaturated with carbon, (□) not saturated with carbon. $\theta_{Al_2O_3}$ and $\theta_{CV}$ indicate the values of equilibrium contact angles on $Al_2O_3$ and $C_V$, respectively

is the contact angle on the unreacted carbon substrate and a final value of $\theta_{eq} \approx 35°$ which is the equilibrium contact angle of the alloy on the reaction product—SiC. The spreading kinetics is governed by the reaction kinetics at the triple line but coupling between reaction and wetting is different before and after $\theta_N$.

Before $\theta_N$ the liquid may directly access the substrate surface ahead of the triple line resulting in a strong coupling and a high spreading rate. For $\theta < \theta_N$ the liquid no longer has direct access to a fresh substrate surface, and as a result coupling is weak and spreading rate decreases strongly [11].

## Effect of different parameters

### *Carbon presaturation of Ni–Si alloy*

An experiment has been carried out with a Ni–63 at.%Si alloy presaturated in carbon. In this case, the Ni–Si alloy is prepared by melting and alloying Ni and Si in a graphite crucible (instead of an alumina crucible) during the experiment. The liquid alloy is maintained for 130 min at 1200 °C before extruding the droplet from the crucible and initiating contact with the carbon coated alumina.

Figure 7 compares the wetting kinetics on carbon-coated alumina for two experiments performed under the same conditions (temperature, mass drop and carbon coating thickness) with and without carbon presaturation of the Ni–63 at.%Ni alloy. Note that for the carbon presaturated alloy, no receding occurs for contact times up to 250 min.

### *Carbon coating layer thickness*

Figure 8 compares the wetting kinetics obtained for two experiments carried out with carbon coating layers differing in thickness by a factor of almost 4 ($e_1 = 18$ nm and $e_2 = 67$ nm). Note that for the thicker carbon layer the

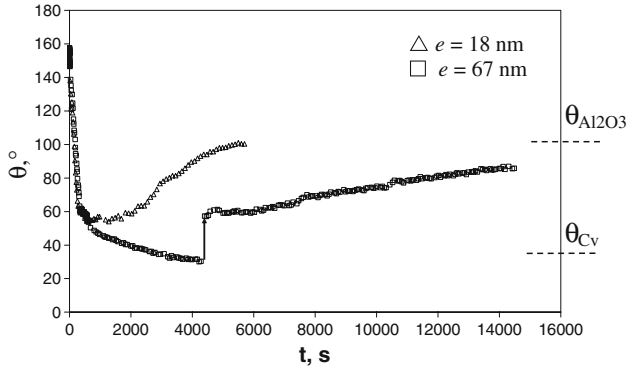


**Fig. 8** Variation in contact angle $\theta$ with time for Ni–63 at.%Si alloy droplets on carbon coated alumina at 1200 °C for two different carbon layer thicknesses

minimum contact angle $\theta_m$ attained is lower and the receding process occurs much later. On the contrary, the carbon layer thickness has no influence on the other characteristic contact angles $\theta_0$ and $\theta_F$.

*Temperature*

Figure 9 presents the $\theta(t)$ curves obtained for three different experiments performed with the same alloy composition, the same mass droplet (m = 33 ± 7 mg) and the same coating thickness ($e$ = 10 ± 3 nm) for three different temperatures. It is found that an increase in temperature leads to an acceleration in spreading kinetics as well as in receding kinetics. As a consequence, the time $t_m$ at which receding starts, corresponding to the minimum of the $\theta(t)$ curve, decreases considerably with temperature: from about 800 s at 1200 °C to 220 s at 1300°.

Note that for an experiment performed at 1150 °C, not presented in Fig. 9, no significant dewetting is observed even after a 12,600 s holding time.

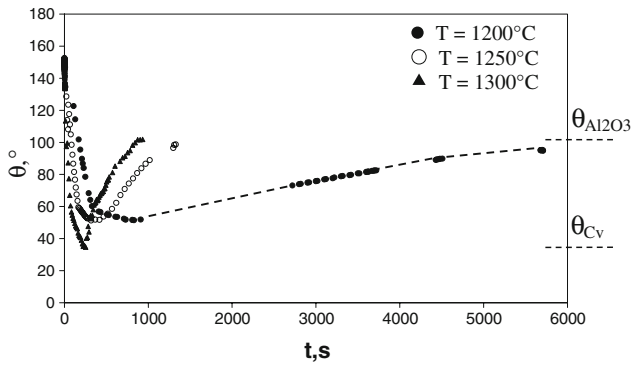


**Fig. 9** Variation in contact angle $\theta$ with time for Ni–63 at.%Si alloy droplets on carbon-coated alumina ($e$ = 10 ± 3 nm) for three different temperatures

*Wetting of Zr–Si alloy*

In order to check the general character of the conclusions drawn in this study (see "Discussion") a further experiment was performed at 1395 °C with the $ZrSi_2$–Si eutectic alloy on sapphire covered by a carbon coating 15 ± 5 nm thick. In this system, the minimum contact angle $\theta_m$ attained after about 60 s is 62° and dewetting starts before reaching the second (slow) spreading stage, i.e. at $\theta > \theta_N$. A final contact angle of 83° is attained in only 140 s. A second experiment carried out with the same composition alloy on non-coated sapphire gives a contact angle of 85 ± 2° in 25 s.

## Discussion

### Drop spreading

From the experimental wetting curves and XPS characterisations, it may be concluded that spreading of the drop on the carbon-coated alumina occurs with the same mechanism as on vitreous carbon, i.e. by lateral extension of the interfacial reaction product (SiC).

Given that the SiC layer formed during spreading of Ni–Si alloy on the bulk vitreous carbon is about 1 μm thick [8], it is concluded that, for all C-coated alumina samples used in this study, the carbon layer (less than 100 nm thick) is completely transformed into SiC.

Spreading occurs in two stages, first rapidly from $\theta_0$ to $\theta_N$ and then very slowly from $\theta_N$ to $\theta_m$. Indeed, the spreading rate around $\theta_N$ changes by one order of magnitude (see Table 1 and "Reference wetting curves" section.).

Table 1 compares the characteristic contact angles, the spreading rates ($U$) and the activation energies of spreading obtained on the C-coated alumina (this study) and on the

**Table 1** Comparison of wetting results of the Ni–63 at.%Si alloy on carbon-coated alumina (this study) and on bulk vitreous carbon [7] at 1200 °C. Activation energy $E_a$ was calculated from results obtained in the temperature range 1150-1300 °C. $U$ ($\theta \geq \theta_N$) and $U$ ($\theta \leq \theta_N$) are the triple line velocities at point N just before and just after the regime change

| | Carbon-coated alumina | Bulk vitreous carbon |
|---|---|---|
| $\theta_0$ (°) | 152 ± 6 | 151 ± 2 |
| $\theta_N$ (°) | 57 ± 3 | 48 |
| $\theta_m$ (°) | 54 − 27 | 35 |
| $U$ ($\theta \geq \theta_N$) μm $s^{-1}$ | 3.5 ± 0.7 | 1.5 |
| $U$ ($\theta \leq \theta_N$) μm $s^{-1}$ | 0.27 ± 0.11 | 0.36 |
| $E_a$ ($\theta > \theta_N$) kJ $mol^{-1}$ | 268 | 255 |
| $E_a$ ($\theta < \theta_N$) kJ $mol^{-1}$ | 443 | 365 |

bulk vitreous carbon substrate obtained by Dezellus et al. [7]. In order to calculate the activation energies, the spreading rate values for the quasi-linear and linear stages at $\theta = \theta_N$ are used. The minimum contact angle $\theta_m$ on vitreous carbon is equal to the equilibrium contact angle on this substrate ($\theta_{eq}$) while $\theta_m$ on C-coated alumina is close to or higher than $\theta_{eq}$. Indeed, on C-coated alumina dewetting can start before reaching the equilibrium contact angle $\theta_{eq}$. The activation energies $E_a$ of reactive spreading on vitreous carbon and on C-coated alumina are comparable. Note that, for $\theta \geq \theta_N$, the spreading rate $U = dR/dt$ on the carbon-coated alumina at 1200 °C is 3–4 μm $s^{-1}$. This value is higher than that obtained on the bulk vitreous carbon (1.5 μm $s^{-1}$) which in turn is about 5 times higher than the spreading rate observed on the bulk graphite $C_{Gr}$ [11], i.e.

$$U(\text{C-coated } Al_2O_3) = 3\text{–}4\,\mu\text{m s}^{-1} > U(C_V) = 1.5\,\mu\text{m s}^{-1} \gg U(C_{Gr})$$

These results strongly suggest that the carbon coating layer structure is much closer to that of vitreous carbon than to graphite. This deduction is logical for a carbon layer obtained by evaporation of a carbon braid and condensation on alumina at room temperature which is expected to be an amorphous layer. Moreover, the experimental temperatures in this study (1150–1300 °C) are too low to enable densification or graphitisation of the carbon layer during the experiments.

## Beyond the triple line

EDX analysis of the film ahead of the triple line showed that this film consists of Ni, Si and C. It can thus be concluded that the film is not unreacted carbon but a mixture of SiC and Ni. This mixture is formed by *reactive infiltration* of liquid Ni–Si in the porous carbon coating layer at time $t$ close to $t_m$, i.e. when the triple line velocity becomes very small. (The mechanism of reactive infiltration of Ni-Si alloys in porous graphite is studied in Ref. [12].) This film is a particular case of *secondary wetting* [1].

## Dewetting and SiC stability

In order to simplify the analysis of the dewetting process, the liquid drop is considered in the first instance to have attained its equilibrium contact angle defined by the equilibrium contact angle on the reaction product SiC ($\theta_{SiC}$). At this moment, at the liquid/solid interface far from the triple line, dissolution of SiC can occur leading to the formation of alumina areas and thus locally transforming an alloy/SiC interface into an alloy/alumina interface (cf. Fig. 10a). When the formation of these alumina areas takes place at the triple line (cf. Fig. 10b), receding of the triple line can occur under the effect of a return force $F$, the value of which per unit length of the triple line is given by the following equation:

$$F = \sigma[\cos\theta_{SiC} - \cos\theta_{Cassie}(\alpha(t))] \quad (1)$$

where $\sigma$ is the liquid–vapour surface energy; $\theta_{Cassie}(\alpha(t))$ is the contact angle on a composite surface consisting of $Al_2O_3$ and SiC areas. This angle is given by the classical Cassie equation

$$\cos\theta_{Cassie}[\alpha(t)] = [1 - \alpha(t)] \cdot \cos\theta_{SiC} + \alpha(t) \cdot \cos\theta_{Al_2O_3} \quad (2)$$

In the case in question, $\alpha(t)$ is the fraction of the triple line which passes through the alumina areas and $\theta_{Al_2O_3}$ is the equilibrium contact angle of liquid on $Al_2O_3$.

Note that drop receding does not necessarily mean that the drop has attained its equilibrium on the carbon layer, i.e. a contact angle $\theta \approx \theta_{SiC}$. Receding in fact becomes possible when the spreading rate becomes low compared to the dissolution rate of the SiC layer. As the spreading rate decreases by about one order of magnitude when $\theta \approx \theta_N$ (see Table 1), the probability of the drop receding strongly increases for $\theta < \theta_N$. The experimental results with

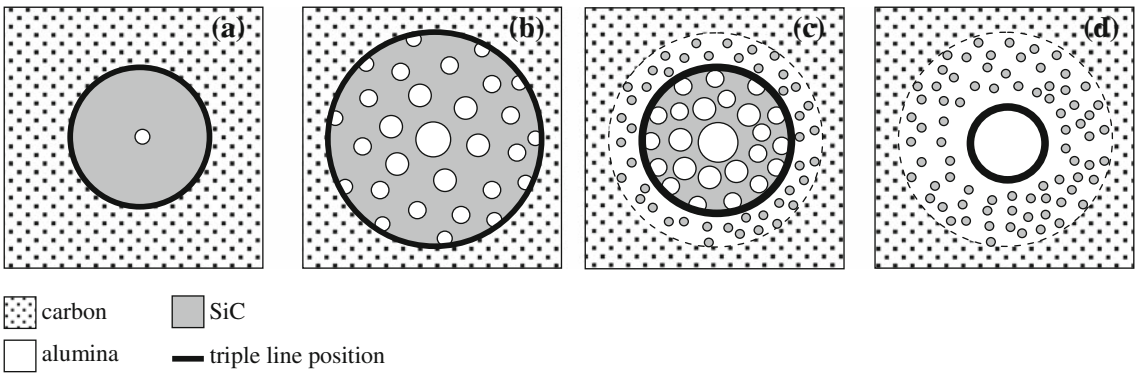


**Fig. 10** Different stages of spreading and receding of the triple line: **a** dissolution of SiC layer far from the triple line leads to the formation of alumina areas (in contact with the liquid), **b** formation of alumina areas takes place at the triple line ($\theta = \theta_m$), **c** receding of the triple line $\theta_m < \theta < \theta_F$, **d** $\theta = \theta_F$

Ni–63 at.%Si alloy show that, when receding takes place, it starts systematically after the break in slope observed on the $R(t)$ curve at $\theta = \theta_N = 57 \pm 3°$. The only exception was for the Zr–Si alloy.

Dewetting is governed by the progress of the dissolution process (i.e. the variation in $\alpha$ as a function of time) and occurs continuously or by jumps (in the case of pinning of the triple line—see Fig. 1) up to $\theta = \theta_{Al_2O_3}$ (Fig. 10d). This explains the presence of Ni–Si droplets (clearly attached on undissolved SiC) inside the dewetting zones situated close to the periphery of the contact surface, while only corrosion lines (rings) of alumina are observed in dewetting areas lying in the central part of the contact surface (see zone BC in Fig. 4).

The kinetic parameter quantifying the stability of the SiC layer at the triple line is the time $t_m$ at which receding starts, i.e. the time corresponding to the minimum of the $\theta(t)$ curve.

In Fig. 11, the neperian logarithm of $t_m$ is plotted versus $1/T$ for experiments performed with the same coating thickness, $e = 10 \pm 3$ nm. The apparent activation energy obtained from the slope of the straight line is $E^* = 335$ kJ mol$^{-1}$. The different contributions to $E^*$ can be evaluated by calculating the dissolution time $t_{diss}$ of a SiC layer of thickness $e$ in the Ni–Si alloy

$$\langle SiC \rangle \rightarrow (Si) + (C) \quad (3)$$

This time is equal to $e/U_{diss}$, where $U_{diss}$ is the dissolution rate.

Assuming that the dissolution rate is limited by the atomic process at the SiC/alloy interface (see "Appendix"), $U_{diss}$ is given by

$$U_{diss} = k\left(C_C^{eq} - C_C\right) \quad (4)$$

$C_C^{eq}$ is the carbon concentration in the Ni–Si alloy in equilibrium with SiC, $C_C$ is the real concentration of carbon in the alloy and $k$ is a kinetic constant.

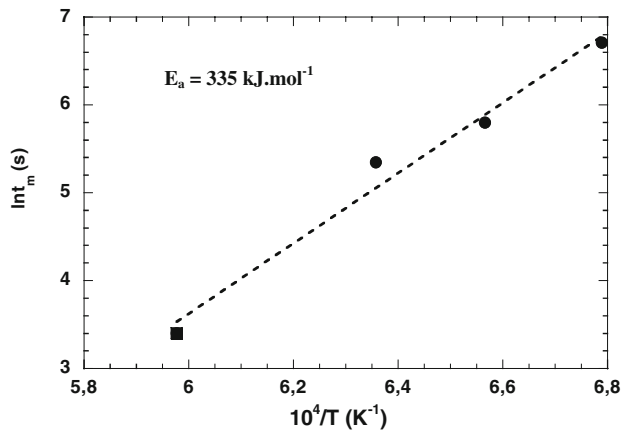


**Fig. 11** Effect of temperature on the time $t_m$ at which the dewetting process starts (■ experiment with a Zr–10 at.%Si alloy)

The calculation of $t_{diss}$ (see "Appendix") leads, for $C_C \ll C_C^{eq}$, to

$$t_{diss} = b \exp\left(\frac{E^*}{RT}\right) \quad (5)$$

where $b$ is a constant. $E^*$ is equal to $E_a + \Delta H°$, $E_a$ being the true activation energy of the dissolution process and $\Delta H°$ is the standard enthalpy of reaction (3) with reference states solid SiC, liquid carbon and liquid silicon. Given that $\Delta H° = 230$ kJ mol$^{-1}$ [13] a value of $E_a = 335–230 = 105$ kJ mol$^{-1}$ is obtained. This value, which is much higher than the activation energy for diffusion in liquid alloys (10–30 kJ mol$^{-1}$ [14]), is compatible with the hypothesis of limitation by the interfacial process.

Note that, at the low temperature, where $C_C^{eq}$ tends towards $C_C$, the dissolution rate tends to zero (see Eq. 4). For a given system, this absolute stability limit is attained when $C_C^{eq}$ becomes close to the concentration of carbon present in the alloy as impurity.

## Conclusions

The contact angle–time curves of molten silicides on C-coated alumina pass through a minimum for a time $t_m$ lying between some tens and a few thousands of seconds, depending on the temperature and coating thickness. At $t < t_m$ the drop wets the substrate with a spreading rate governed by the reaction of formation of silicon carbide at the triple line. At $t > t_m$ dewetting occurs, controlled by the dissolution rate of silicon carbide in the molten silicide. $t_m$ which can be considered as a measure of the lifetime of a liquid alloy deposited on coated alumina, decreases with temperature exponentially with a high apparent activation energy (335 kJ mol$^{-1}$). At low temperature the absolute stability limit of the liquid film is attained when the equilibrium concentration of the carbon in the alloy becomes close to the concentration of carbon contained in the initial alloy as an impurity or introduced into it from the furnace atmosphere.

## Appendix: Calculation of the dissolution rate of an SiC layer in the Ni–Si alloy

This calculation is performed assuming that the dissolution rate ($U_{diss}$) of a SiC layer of thickness $e$ in the Ni–Si alloy:

$$\langle SiC \rangle \rightarrow (Si) + (C) \quad (6)$$

is limited by the atomic process at the SiC/alloy interface.

In this case, the driving force of dissolution is equal to the difference between the chemical potential of carbon in SiC (equal to the chemical potential of the carbon in a

liquid alloy in equilibrium with SiC, corresponding to $C_C^{eq}$) and the actual chemical potential of carbon in the bulk liquid (corresponding to $C_C$). The chemical potential of carbon in SiC and in the bulk liquid is referred to pure liquid carbon. Therefore, $U_{diss}$ is given by

$$U_{diss} = k\left(C_C^{eq} - C_C\right) \tag{7}$$

where $k$ is a kinetic constant which is expressed classically as a function of temperature by

$$k = k_0 \exp\left(-\frac{E_a}{RT}\right) \tag{8}$$

$E_a$ being the activation energy of the dissolution process.

The concentration $C_C^{eq}$ is related to the standard Gibbs energy ($\Delta G°$) of the dissolution reaction (6) (with reference states solid SiC, liquid Si and liquid C), by

$$C_C^{eq} = \frac{V_m}{a_{Si}\gamma_C^{\infty}} \exp\left(-\frac{\Delta G^{\circ}}{RT}\right) \tag{9}$$

where $V_m$ is the molar volume of the liquid alloy and $a_{Si}$ is the activity of silicon in the Ni–Si alloy. $\gamma_C^{\infty}$ is the activity coefficient of carbon at infinite dilution in Ni–Si alloy (activities of Si and C are referred to pure liquids Si and C, respectively). The last quantity is related to the partial enthalpy $\Delta\overline{H}_C^{\infty}$ and excess entropy of mixing $\Delta\overline{S}_C^{xs,\infty}$ of carbon in the alloy by

$$\gamma_C^{\infty} = \exp\left(\frac{\Delta\overline{H}_C^{\infty} - T\Delta\overline{S}_C^{xs,\infty}}{RT}\right) \tag{10}$$

As for $\Delta G°$, it is related to the standard dissolution enthalpy $\Delta H°$ and entropy $\Delta S°$ by: $\Delta G° = \Delta H° - T\Delta S°$, therefore,

$$C_C^{eq} = m \exp\left(-\frac{\Delta H^{\circ} + \Delta\overline{H}_C^{\infty}}{RT}\right) \quad \text{with}$$
$$m = \frac{V_m}{a_{Si}} \exp\left(\frac{\Delta S^{\circ} + \Delta\overline{S}_C^{xs,\infty}}{R}\right) \tag{11}$$

Then, taking into account that the dissolution time $t_{diss}$ is equal to $e/U_{diss}$, the following expression for $t_{diss}$ is obtained for $C_C \ll C_C^{eq}$:

$$t_{diss} = b \exp\left(\frac{E^*}{RT}\right) \tag{12}$$

where $b = (ek_0)/m$ is a constant and $E^* = E_a + \Delta H^{\circ} + \Delta\overline{H}_C^{\infty}$ is the apparent activation energy of the process. The partial enthalpy of mixing of carbon in the Ni–63 at.%Si alloy at infinite dilution is given by [15]

$$\Delta\overline{H}_C^{\infty} = x_{Ni}\Delta\overline{H}_{(C)_{Ni}}^{\infty} + x_{Si}\Delta\overline{H}_{(C)_{Si}}^{\infty} - \Delta_m H_{(Ni,Si)} \tag{13}$$

The enthalpy of mixing of Ni–Si alloy, $\Delta_m H_{(Ni,Si)}$, can be represented as a function of the mole fractions and the exchange energy $\lambda_{Ni-Si}$ of the Ni–Si solution by considering this alloy as a regular solution $\Delta_m H_{(Ni,Si)} = \lambda_{Ni-Si} x_{Ni} x_{Si}$. The application of Eq. 13 with $\Delta\overline{H}_{(C)_{Ni}}^{\infty} = -110$ kJ mol$^{-1}$ [16], $\Delta\overline{H}_{(C)_{Si}}^{\infty} = 25$ kJ mol$^{-1}$ [16] and $\lambda_{Ni-Si} = -103$ kJ mol$^{-1}$ [17] leads to $\Delta\overline{H}_C^{\infty} \approx 0$. In this case, the apparent activation energy becomes $E^* \approx E_a + \Delta H^{\circ}$.

## References


1. Eustathopoulos N, Nicholas M, Drevet B (1999) Wettability at high temperatures. Pergamon Materials Series v.3 Pergamon, Oxford
2. Koltsov A, Hodaj F, Eustathopoulos N (2008) Mater Sci Eng 495A:259
3. John H, Hausner H (1986) Int J High Technol Ceram 2:73
4. Weirauch DA Jr, Krafick WJ (1990) Metall Trans A 21(6):1745
5. Sobczak N, Nowak R, Radziwill W, Kudyba A, Wojciechowski A, Rudnik D (2005) Ceramika/Ceramics 80:669
6. Rado C (1997) Thèse INP Grenoble, France
7. Dezellus O, Hodaj F, Eustathopoulos N (2002) Acta Mater 50:4741
8. Bougiouri V, Voytovych R, Dezellus O, Eustathopoulos N (2007) J Mater Sci 42:2016. doi:10.1007/s10853-006-1483-8
9. Waldrop JR, Grant RW (1990) Appl Phys Lett 56:557
10. Koltsov A (2005) Ph.D. Thesis, Institut National Polytechnique de Grenoble, France
11. Dezellus O (2000) Ph.D. Thesis, Institut National Polytechnique de Grenoble, France
12. Voytovych R, Bougiouri V, Calderon NR, Narciso J, Eustathopoulos N (2008) Acta Mater 56:2237
13. Chase MW (1998) NIST-JANAF thermochemical tables, 4th edn. J Phys Chem Ref Data, Monograph 9, Amer Chem Soc and Amer Inst of Physics, New York
14. Geiger GH, Poirier DR (1980) Transport phenomena in metallurgy, Adison-Wesley Series in metallurgy and materials. Adison-Wesley Publishing Company, MA
15. Kubashewski O, Alcock CB, Spencer PJ (1993) Materials thermochemistry, 6th edn. Pergamon Press, NY
16. Du Y, Schuster JC (1999) Metall Mater Trans A 30A:2409
17. An Mey S (1986) Z Metallkd 77(12):805